

## Does deamidation of islet amyloid polypeptide accelerate amyloid fibril formation?

Lam, Yuko P. Y.; Wootton, Christopher A.; Hands-portman, Ian J.; Wei, Juan; Chiu, Cookson K. C.; Romero-Canelón, Isolda; Lermyte, Frederik; Barrow, Mark P.; O'connor, Peter B.

DOI:  
[10.1039/C8CC06675B](https://doi.org/10.1039/C8CC06675B)

License:  
None: All rights reserved

Document Version  
Peer reviewed version

Citation for published version (Harvard):  
Lam, YPY, Wootton, CA, Hands-portman, IJ, Wei, J, Chiu, CKC, Romero-Canelón, I, Lermyte, F, Barrow, MP & O'connor, PB 2018, 'Does deamidation of islet amyloid polypeptide accelerate amyloid fibril formation?', *Chemical Communications*, vol. 54, no. 98, pp. 13853-13856. <https://doi.org/10.1039/C8CC06675B>

[Link to publication on Research at Birmingham portal](#)

**Publisher Rights Statement:**  
Checked for eligibility 07/12/2018

This is a peer-reviewed version of an article published in Chemical Communications.  
Chem. Commun., 2018,54, 13853-13856  
[10.1039/C8CC06675B](https://doi.org/10.1039/C8CC06675B)

### General rights

Unless a licence is specified above, all rights (including copyright and moral rights) in this document are retained by the authors and/or the copyright holders. The express permission of the copyright holder must be obtained for any use of this material other than for purposes permitted by law.

- Users may freely distribute the URL that is used to identify this publication.
- Users may download and/or print one copy of the publication from the University of Birmingham research portal for the purpose of private study or non-commercial research.
- User may use extracts from the document in line with the concept of 'fair dealing' under the Copyright, Designs and Patents Act 1988 (?)
- Users may not further distribute the material nor use it for the purposes of commercial gain.

Where a licence is displayed above, please note the terms and conditions of the licence govern your use of this document.

When citing, please reference the published version.

### Take down policy

While the University of Birmingham exercises care and attention in making items available there are rare occasions when an item has been uploaded in error or has been deemed to be commercially or otherwise sensitive.

If you believe that this is the case for this document, please contact [UBIRA@lists.bham.ac.uk](mailto:UBIRA@lists.bham.ac.uk) providing details and we will remove access to the work immediately and investigate.

# Does Deamidation of Islet Amyloid Polypeptide Accelerate Amyloid Fibril Formation?

Yuko P. Y. Lam,<sup>a</sup> Christopher A. Wootton,<sup>a</sup> Ian Hands-Portman,<sup>b</sup> Juan Wei,<sup>a</sup> Cookson K. C. Chiu,<sup>a</sup> I. Romero-Canelon,<sup>ac</sup> Frederik Lermyte,<sup>a</sup> Mark P. Barrow,<sup>a</sup> Peter B. O'Connor\*<sup>a</sup>

## Abstract

Mass spectrometry has been applied to determine the deamidation sites and the aggregation region of the deamidated human islet amyloid polypeptide (hIAPP). Mutant hIAPP with iso-aspartic residue mutations at possible deamidation sites showed very different fibril formation behavior, which correlates with the observed deamidation-induced acceleration of hIAPP aggregation.

Deamidation is a non-enzymatic post-translational modification (PTM) which contributes to protein ageing.<sup>1</sup> Deamidation occurs spontaneously in solution at asparagine (Asn) and glutamine (Gln) residues, and results in formation of iso-aspartic acid/aspartic acid and  $\gamma$ -glutamic acid/glutamic acid (and their stereoisomers), respectively.<sup>2,3</sup> The deamidation rate of Asn is faster than Gln due to the shorter distance between the main chain amido group (-NH-) and the side chain amide group (-NH<sub>2</sub>-).<sup>4,5</sup> With an additional methylene group (-CH<sub>2</sub>-) into the backbone of iso-aspartic acid and  $\gamma$ -glutamic acid; the tertiary structure, stability, folding, and function of proteins can be dramatically altered by deamidation.<sup>6,7</sup> Previous studies showed that deamidation can accelerate fibril formation in certain cases, including mutated amyloid- $\beta$  (D7N and D23N) observed in Alzheimer's disease.<sup>8,9</sup> Aggregation of  $\beta_2$ -microglobulin from dialysis-associated amyloidosis disease,<sup>10,11</sup> and  $\alpha$ B-crystallin from human eye lens have also been shown to be affected by deamidation.<sup>12,13</sup>

Human islet amyloid polypeptide (hIAPP; also referred to as amylin) is a 37-residue hormone peptide co-secreted with insulin and involved in regulating blood glucose levels.<sup>14</sup> The concentration of hIAPP is around 1-2% relative to the level of insulin in secretory granules.<sup>15</sup> hIAPP contains an intramolecular disulfide bond between Cys-2 and Cys-7, as well as an amidated C-terminus,<sup>16</sup> and is an intrinsically disordered protein with a low level of persistent helical structure between residues Asn-3 and Leu-27 in solution.<sup>17</sup> hIAPP is an amyloid protein which contains six Asn and one Gln as potential deamidation sites. A previous study from Nilsson *et al.* used a variant of hIAPP segment, residues 20-29 (SNNFPAILSS) which is

non-amyloidogenic and showed that addition of less than 5% of deamidated monomer could accelerate the amyloid fibril formation.<sup>18</sup> Results from Dunkelberger *et al.* also showed that deamidation of hIAPP disrupted the  $\beta$ -sheet structure around Leu-27, resulting in a morphology change of hIAPP fibrils, along with accelerated fibril formation.<sup>19</sup> The formation of hIAPP fibrils does not contribute to type II diabetes (T2D); however early oligomers of hIAPP lead to the decline of pancreatic  $\beta$ -cell mass and the failure of islet cell transplantation for T2D treatment.<sup>20-22</sup> Thus, accelerating the formation of the early oligomers of hIAPP may reduce the graft survival rate.<sup>17, 23</sup> Deamidation has a significant impact on hIAPP fibril formation,<sup>24, 25</sup> the effects on the deamidation rate, the deamidation site(s), and the effects of isomeric deamidation products of hIAPP, however, have not yet been fully addressed.

MS is a powerful tool for examining deamidation in proteins as the deamidation reaction produces products with a mass shift of +0.984 Da ( $-\text{NH}_2$  to  $-\text{OH}$ ) at the deamidated residue, which is readily detected by MS.<sup>26-28</sup> Previous studies also suggested that deamidation can be directly quantified by measuring the peak area of the non-deamidated and deamidated peaks, thus the percentage of deamidation in the sample can be estimated.<sup>29, 30</sup> Tandem MS/MS can further locate the deamidation site in proteins, and differentiate the isomeric deamidation products.<sup>2, 26-30</sup> Collisionally activated dissociation (CAD) MS/MS can localise deamidation site via a mass shift (+0.984 Da) appears in b and y ion fragments containing the deamidated residue, while unmodified fragments are observed in the regions not containing deamidated residues.<sup>30</sup> Electron capture dissociation (ECD) MS/MS can be used to not only localises the deamidation site in protein, but also uses to differentiate the isomeric products of deamidation by the mass shift of +58 and -57 Da at the c and z ion fragments of iso-/ $\gamma$ - deamidation products respectively. The peak intensity of iso-/ $\gamma$ - deamidation products can also compare with the peak intensity of aspartic acid/glutamic acid in order to determine the ratio of the isomeric products.<sup>29</sup>

In order to localise the deamidation site(s) in the incubated hIAPP solution, CAD MS/MS with a 12 Tesla (T) Fourier transform ion cyclotron mass spectrometer (FTICR MS) was applied. The  $y_5$  fragment clearly showed a deamidated peak in the incubated sample (Fig. 1B), indicating deamidation occurs at Asn-35 residue in hIAPP. For the b fragments, no deamidated peaks were observed for the first 20 amino acid residues (Fig. 1C); however, a deamidated peak was present corresponding to the  $b_{21}$  fragment (Fig. 1D), suggesting deamidation only occurs at Asn-21 but not at Asn-3, Gln-10, and Asn-14 residues. Furthermore, another deamidated peak was detected corresponding to the  $b_{22}$  fragment ion in the incubated solution (Fig. 1E), indicating Asn-22 also deamidates within four weeks at 37°C.

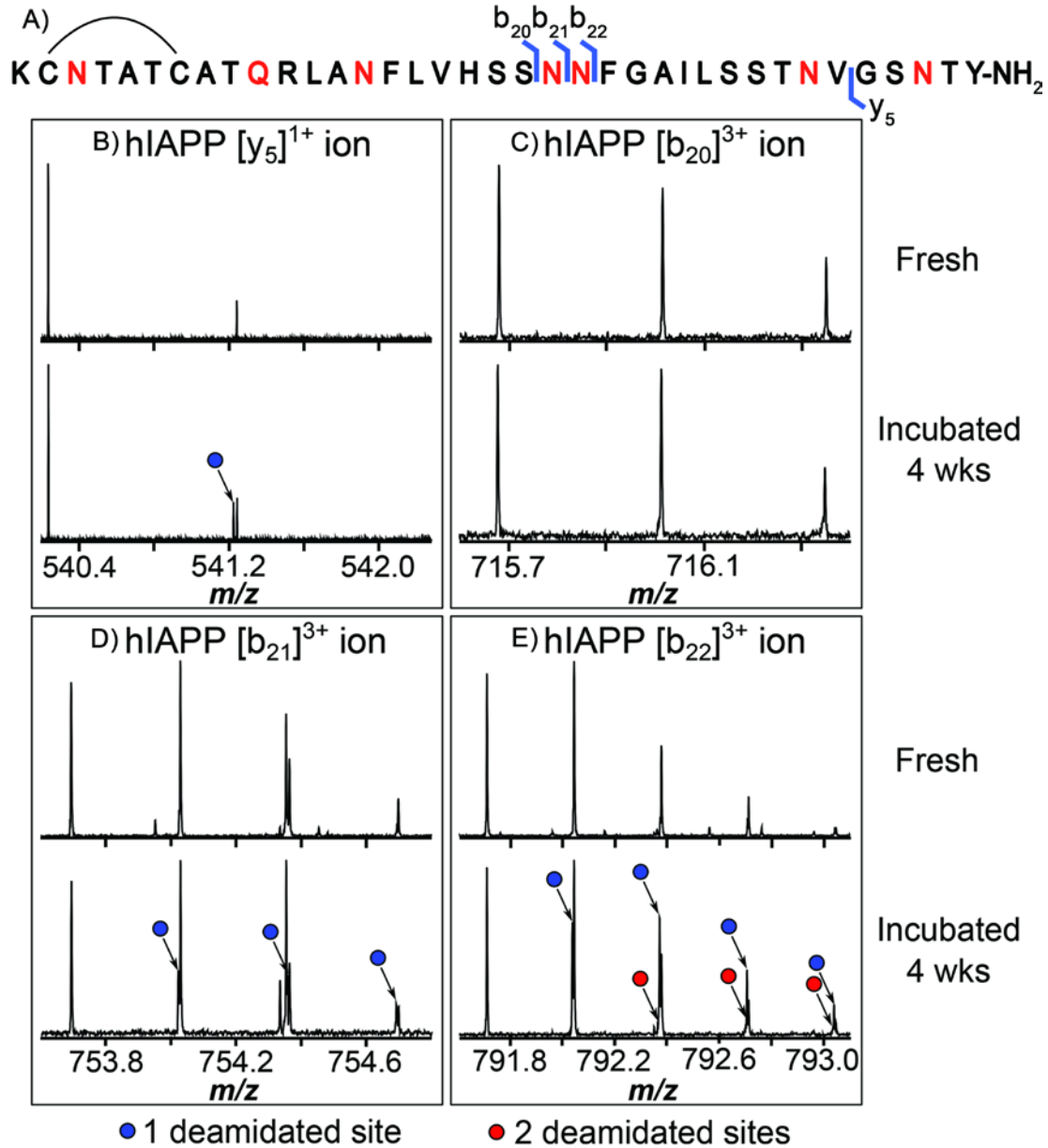


**Figure 1.** (A) The amino acid sequence of hIAPP. The potential deamidation sites are coloured in red. Key CAD MS/MS fragments of hIAPP revealing deamidation at amino acid residues after 4 weeks incubation at 37°C are shown (B)  $y_5$ , (C)  $b_{20}$ , (D)  $b_{21}$ , and (E)  $b_{22}$ . The blue/red circles indicate the isotopic peaks of singly/doubly deamidated fragments, respectively.

Subsequently, MS was applied to determine the deamidation rates of each individual deamidated site in the incubated solutions and resulting fibrils by calculating the percentage ratio between the non-deamidated and the deamidated fragment ion peak areas for each sample. In the incubated solution, the earliest deamidation instance was observed on day 5, and was identified within the  $y_5$  fragment ion (Fig. 2A), indicating the Asn-35 is the first amino acid residue in hIAPP to undergo deamidation, which requires 5-day of incubation at 37°C. Deamidation at

the  $b_{21}$  and  $b_{22}$  fragment ions was observed on day 8, suggesting Asn-21 and Asn-22 residues are the next amino acid residue to deamidate in hIAPP and require a longer incubation time for deamidation compared to Asn-35 residue. Though the extent of deamidation increased with the incubation time; a similar percentage and rate of deamidation were found in the  $y_5$ ,  $b_{21}$ , and  $b_{22}$  fragment ions at the various time points for the incubated solutions. After 28 days incubation, each deamidated fragment ion ( $y_5$ ,  $b_{21}$ , and  $b_{22}$ ) of the soluble hIAPP showed ~18% deamidation, indicating even though the initial deamidation time between Asn-21, Asn-22, and Asn-35 residues are different, the extent as well as the rate of deamidation of these residues are similar across and at the end of the incubation time. The insoluble protein pellets formed over the course of the incubation were re-solubilised and showed a greater extent of deamidation than the soluble hIAPP species. Deamidation was observed in the day-7, day-14, day-21, and day-28 samples (Fig. 2B). On day-7, ~7.5% of the  $y_5$  fragment ion was deamidated while no deamidation was observed for the  $b_{21}$  and  $b_{22}$  fragment ions in the pellet. On day-14, the extent of deamidation for the  $y_5$  fragment ion increased sharply to 16% and the  $b_{21}$  and  $b_{22}$  showed ~7.5% deamidation. After 28 days incubation, the extent of deamidation of the  $y_5$ ,  $b_{21}$ , and  $b_{22}$  fragment ions were at 39%, 30%, and 29% respectively, distinctly larger than for the soluble hIAPP species above, suggesting the fibrils of hIAPP contains a higher extent of deamidation at Asn-35 compared to Asn-21 and Asn-22 residues. The residue Asn-35 was the earliest deamidation site observed in the incubated solutions and contained the highest extent of deamidation in the fibril pellets, which agrees with the findings in previous deamidation studies,<sup>3,31</sup> suggesting that the primary sequence of Ser-<sup>35</sup>Asn-Thr in hIAPP had the shortest deamidation time among all the other segments studied. The higher extent of deamidation observed in the fibrils of hIAPP compared to the incubated solutions also indicates that deamidated hIAPP tends to aggregate and form insoluble fibrils more rapidly than the wild-type hIAPP.

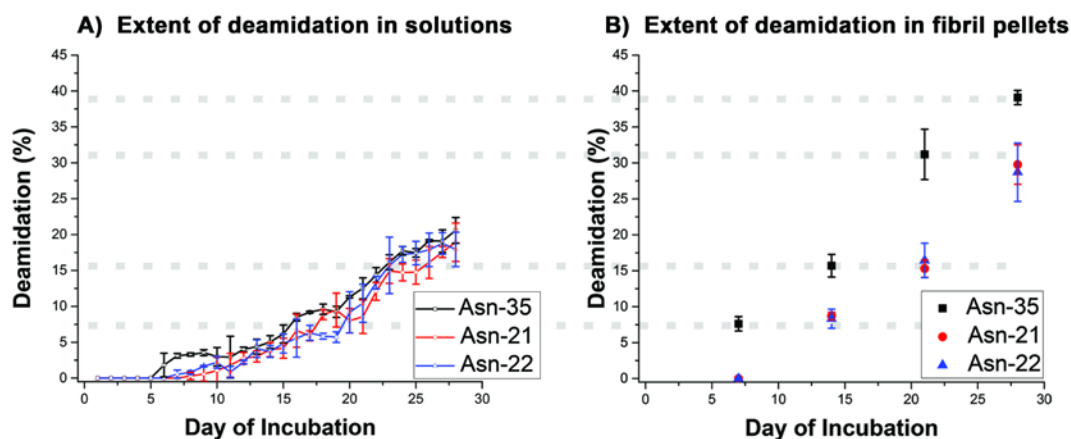


**Figure 2.** The extent of deamidation observed in CAD MS/MS fragments; the  $y_5$  (black),  $b_{21}$  (red), and

b<sub>22</sub> (blue) for 10  $\mu$ M aqueous hIAPP (A) solutions and (B) dissolved fibril solutions.

In order to ascertain the effects of deamidated isomeric products on the aggregation process, pure mutant hIAPP peptides were synthesised with aspartic acid ((D)<sub>3</sub>hIAPP) or iso-aspartic acid ((isoD)<sub>3</sub>hIAPP) replacement at the detected deamidation site from above, i.e. residues 21, 22, and 35 (Fig. S1, ESI<sup>†</sup>). The 7+ charge state dimers of ((D)<sub>3</sub>hIAPP) and ((isoD)<sub>3</sub>hIAPP) were fragmented by ECD MS/MS in order to determine the non-covalent interaction region between the mutant hIAPP units (Fig. S2 – S3, ESI<sup>†</sup>). The aggregation regions of ((D)<sub>3</sub>hIAPP) and ((isoD)<sub>3</sub>hIAPP) were found between Asn-31 and Thr-36 residues, which is similar to the proposed aggregation region of 7+ charge state dimer of wild-type hIAPP in the previous studies, suggesting there is no difference between the wild-type and the two mutant hIAPPs regarding the aggregation sites for the formation of early oligomers.<sup>32</sup>

MS can quantify soluble amyloid proteins in solution.<sup>32</sup> The ionisation of aqueous protein solutions to gas phase ions, however, is limited to soluble components only, so that the insoluble fibrils are difficult to quantify using MS. Thus, the relative concentration of amyloid fibrils formed in the incubated solutions were determined by using Thioflavin T (ThT) fluorescence emission analysis at the wavelength of 490 nm and the overall structures of fibrils were observed using transmission electron microscopy (TEM). The relative fluorescence emission of the 10  $\mu$ M solutions of wild-type hIAPP, ((D)<sub>3</sub>hIAPP), and ((isoD)<sub>3</sub>hIAPP) were measured and the lag phases of the formation of mature fibrils in wild-type hIAPP solution was 42 hours while in ((D)<sub>3</sub>hIAPP) and ((isoD)<sub>3</sub>hIAPP) solutions were ~ 30 hours (Fig. 3A – 3C), indicating mutant hIAPPs with deamidated residues replacement at Asn-21, Asn-22, and Asn-35 accelerate the rate of mature fibrils formation which supports the hypothesis that deamidated hIAPPs accelerate the aggregation rate of non-deamidated hIAPP.<sup>18, 19</sup> TEM images of the wild-type hIAPP, ((D)<sub>3</sub>hIAPP), and ((isoD)<sub>3</sub>hIAPP) solutions incubated at 37°C for one week were also obtained (Fig. 3E – 3G). Branched and elongated fibrils were observed in the wild-type hIAPP as well as ((D)<sub>3</sub>hIAPP) incubated solutions; while densely packed fibrils were found in ((isoD)<sub>3</sub>hIAPP) solution. The fibril structures observed in ((isoD)<sub>3</sub>hIAPP) solution were distinctly different from the fibrils found in wild-type hIAPP and ((D)<sub>3</sub>hIAPP), suggesting the morphology of fibrils formed in ((isoD)<sub>3</sub>hIAPP) is different from wild-type hIAPP as well as ((D)<sub>3</sub>hIAPP).

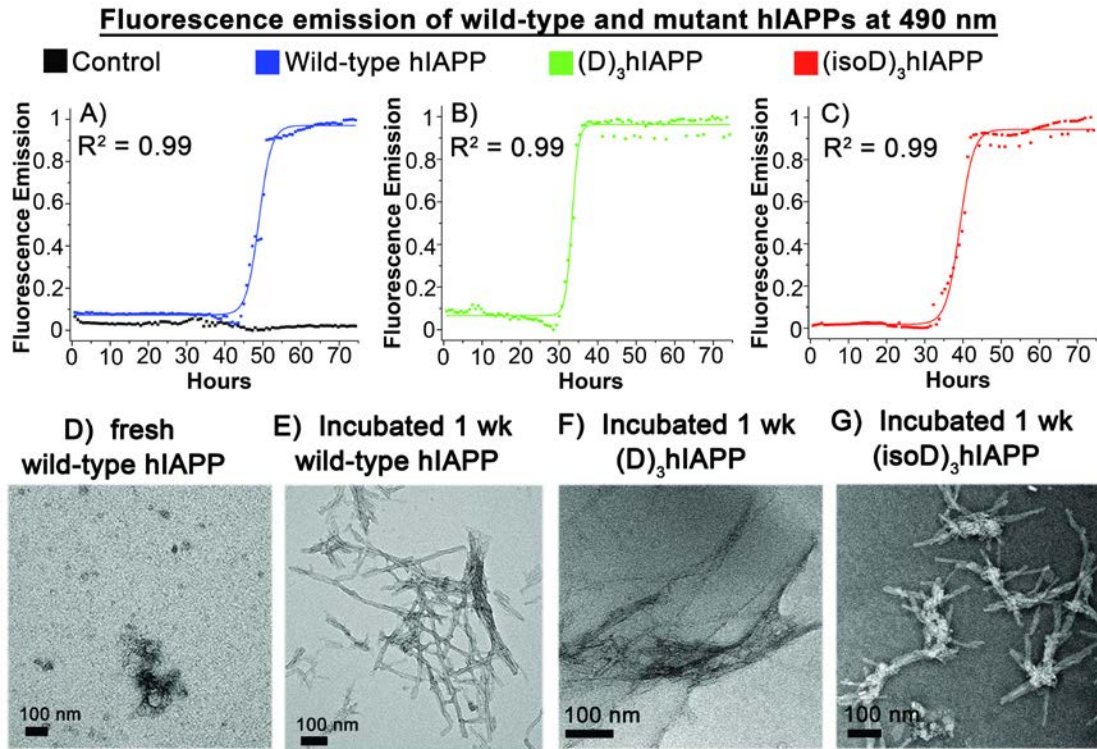


**Figure 3.** The relative fluorescence activity of the incubated 10  $\mu$ M (A) ThT solution (control; black), 10  $\mu$ M wild-type hIAPP (blue), (B) 10  $\mu$ M mutant ((D)<sub>3</sub>hIAPP) (green), and (C) 10  $\mu$ M mutant ((isoD)<sub>3</sub>hIAPP) (red) solutions measured at emission 490 nm. The TEM images of the (D) fresh and (E) 1-week incubated 10  $\mu$ M wild-type hIAPP solutions. The TEM images of 10  $\mu$ M (F) ((D)<sub>3</sub>hIAPP) and (G) ((isoD)<sub>3</sub>hIAPP) solutions after 1 week incubation at 37°C. The scale bars for each TEM image are inset.

In order to study the effects of the isomeric deamidation products on the wild-type hIAPP aggregation, ((D)<sub>3</sub>hIAPP) and ((isoD)<sub>3</sub>hIAPP) solutions were individually spiked into wild-type hIAPP solution at 5%, 10%, 25%, and 50% amounts. After one week incubation, the percentage of remaining soluble monomeric hIAPP in the seeded solutions was consistently less in the spiked solutions than the control hIAPP incubated solution, and less soluble hIAPP was found in the mutant ((isoD)<sub>3</sub>hIAPP) spiked solutions compared to the ((D)<sub>3</sub>hIAPP) spiked solutions (Fig. 4A). The p-values of seeding 5% and 10% mutant ((D)<sub>3</sub>hIAPP) into the solution were higher than 0.05, which indicated the differences between the seeded solutions and the control sample were not significant. The p-values of the remaining seeded solutions were less than 0.05, which showed significant differences between the control and the seeded solutions. The normalised percentage of soluble hIAPP with 5% spiking of ((D)<sub>3</sub>hIAPP) or ((isoD)<sub>3</sub>hIAPP) was 4% and 9% less than the soluble hIAPP found in the control incubated solutions respectively. The normalised percentage of soluble hIAPP consistently decreased with increased



amounts of ((D)<sub>3</sub>hIAPP) or ((isoD)<sub>3</sub>hIAPP) in the incubated solutions. For the solutions with 50% spiking of ((D)<sub>3</sub>hIAPP) or ((isoD)<sub>3</sub>hIAPP), the normalised percentage of soluble hIAPP was 28% and 46% less than the soluble hIAPP found in the control solutions respectively. These results indicate the effects of mutant hIAPPs in accelerating wild-type hIAPP are concentration-dependent.

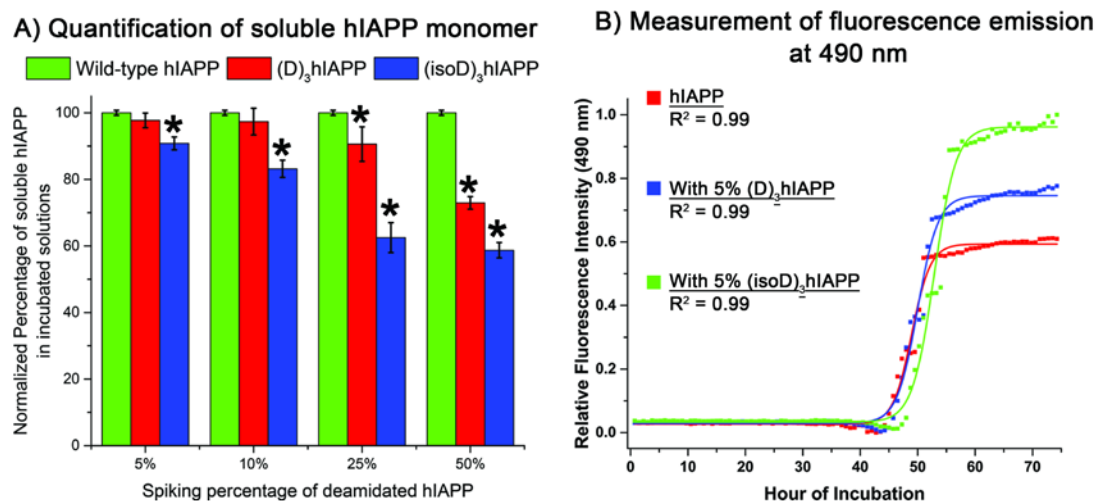


**Figure 4.** (A) A plot showing the normalised percentage of soluble hIAPP in the 10  $\mu$ M solutions with spiking different percentage of mutant ((D)<sub>3</sub>hIAPP) or ((isoD)<sub>3</sub>hIAPP) to wild-type hIAPP (control) measured using MS after 1 week incubation. \* indicates the p-value of the sample percentages are less than 0.05 compared to the control percentage in a paired t-test. (D) The relative fluorescence activity of 10  $\mu$ M hIAPP, 9.5  $\mu$ M hIAPP plus 0.5  $\mu$ M (5%) ((D)<sub>3</sub>hIAPP), and 9.5  $\mu$ M hIAPP plus 0.5  $\mu$ M (5%) ((isoD)<sub>3</sub>hIAPP) measured at emission 490 nm.

The fibrils formed during the incubation experiments were measured using ThT fluorescence spectroscopy. The measured percentage change of fluorescence emission in 5% mutant hIAPP seeded solutions further indicated that the amount of amyloid fibrils formed in the seeded solutions were consistently higher than the wild-type hIAPP incubated solution and the overall percentage of amyloid fibrils formed in ((D)<sub>3</sub>hIAPP) and ((isoD)<sub>3</sub>hIAPP) seeded solutions was 27% and 48% higher than the wild-type hIAPP incubated solution respectively (Fig. 4B). The fluorescence emission measurement and MS quantification showed the effect of seeding ((isoD)<sub>3</sub>hIAPP) is twice that of seeding the same amount of ((D)<sub>3</sub>hIAPP) into non-deamidated hIAPP solutions. The difference between the TEM images of incubated ((D)<sub>3</sub>hIAPP) and ((isoD)<sub>3</sub>hIAPP) solutions also agrees the greater effect of ((isoD)<sub>3</sub>hIAPP) compared to ((D)<sub>3</sub>hIAPP) (Fig. 3E – 3G). The observed morphology of fibrils was different in ((isoD)<sub>3</sub>hIAPP) compared to ((D)<sub>3</sub>hIAPP), indicating differences in the aggregation behaviour and rate of non-deamidated hIAPP, as observed in the MS and fluorescence.



In order to examine the effects of mutant ((D)<sub>3</sub>hIAPP) and ((isoD)<sub>3</sub>hIAPP) in incubated solutions and fibrillary pellets, MS spectra of mixed wild-type hIAPP with various spiking percentage of mutant ((D)<sub>3</sub>hIAPP) and ((isoD)<sub>3</sub>hIAPP) were acquired (Fig. S4, ESI<sup>†</sup>). The peak intensity of mutant ((D)<sub>3</sub>hIAPP) and ((isoD)<sub>3</sub>hIAPP) were consistently higher in the fibrillary pellets compared to the incubated and the fresh solutions, suggesting the important role of ((D)<sub>3</sub>hIAPP) or ((isoD)<sub>3</sub>hIAPP) in enhancing fibril formation.

The experimental results herein demonstrate the importance as well as the effects of hIAPP deamidation on hIAPP aggregation rate. Deamidation of hIAPP is shown to occur at Asn-21, Asn-22, as well as Asn-35 residues of the incubation and a higher percentage of deamidated hIAPP was observed in fibrillary pellet, suggesting that deamidated hIAPP can accelerate the rate of hIAPP fibril formation. The experimental results of the mutant hIAPP, ((D)<sub>3</sub>hIAPP) and ((isoD)<sub>3</sub>hIAPP), not only agree with the hypothesis of deamidated hIAPP can increase fibril formation, but also suggest the effect of seeding ((isoD)<sub>3</sub>hIAPP) is twice than that of ((D)<sub>3</sub>hIAPP) seeding into non-deamidated hIAPP solutions as the morphology of ((isoD)<sub>3</sub>hIAPP) fibrils are distinctly different from the fibrils formed in ((D)<sub>3</sub>hIAPP) solutions. These results provide qualitative and quantitative evaluation of deamidated hIAPP on the rate of aggregation which could help inform further studies of the effects of deamidation on accelerating amyloid fibril formation.

### Conflicts of interest

There are no conflicts to declare.

### Acknowledgements

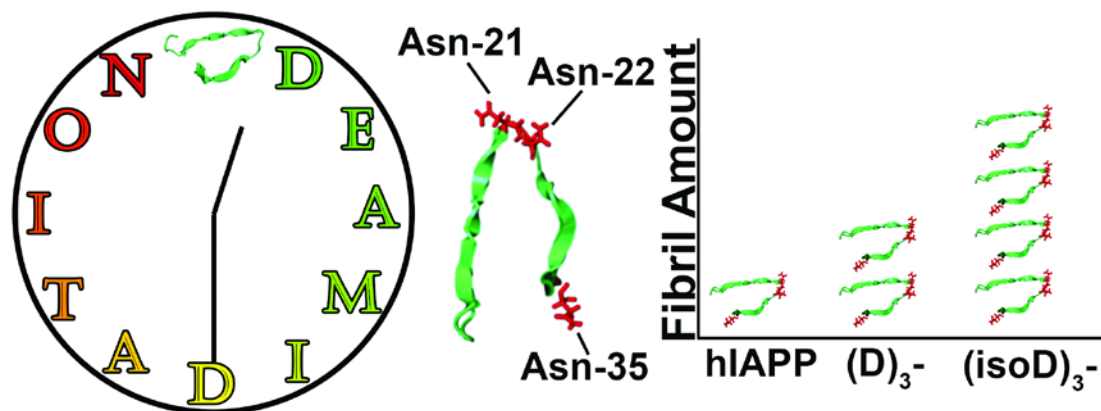
This research was supported by the funding from University of Warwick Research Development Fund (RD16003), Engineering and Physical Sciences Research Council (EP/F034210/1, EP/J000302/1, EP/N021630/1), Funds for Women Graduates, and Great Britain China Centre.

### References

1. E. R. Stadtman, *J. Gerontol.*, 1988, **43**, B112-B120.
2. J. J. Cournoyer, J. L. Pittman, V. B. Ivleva, E. Fallows, L. Waskell, C. E. Costello and P. B. O'Connor, *Protein Sci.*, 2005, **14**, 452-463.
3. N. E. Robinson and A. B. Robinson, *Proc. Natl. Acad. Sci. USA*, 2001, **98**, 944-949.
4. A. B. Robinson and C. J. Rudd, *Curr. Top. Cell. Regul.*, 1974, **8**, 247-295.
5. H. T. Wright, *Crit. Rev. Biochem. Mol. Biol.*, 1990, **26**, 1-52.

6. H. A. Doyle and M. J. Mamula, *Trends Immunol.*, 2001, **22**, 443-449.
7. N. E. Robinson and A. Robinson, *Molecular clocks: deamidation of asparaginyl and glutaminyl residues in peptides and proteins*, Althouse press, Oregon, 2004.
8. N. P. Sargaeva, C. Lin and P. B. O'Connor, *Anal. Chem.*, 2011, **83**, 6675-6682.
9. T. Shimizu, H. Fukuda, S. Murayama, N. Izumiyama and T. Shirasawa, *J. Neurosci. Res.*, 2002, **70**, 451-461.
10. N. M. Kad, N. H. Thomson, D. P. Smith, D. A. Smith and S. E. Radford, *J. Mol. Biol.*, 2001, **313**, 559-571.
11. A. J. Soulby, J. W. Heal, M. P. Barrow, R. A. Roemer and P. B. O'Connor, *Protein Sci.*, 2015, **24**, 850-860.
12. R. Gupta and O. P. Srivastava, *Invest. Ophthalmol. Vis. Sci.*, 2004, **45**, 206-214.
13. T. Takata, J. T. Oxford, B. Demeler and K. J. Lampi, *Protein Sci.*, 2008, **17**, 1565-1575.
14. G. J. S. Cooper, A. J. Day, A. C. Willis, A. N. Roberts, K. B. M. Reid and B. Leighton, *Biochim. Biophys. Acta*, 1989, **1014**, 247-258.
15. E. Jaikaran, M. R. Nilsson and A. Clark, *Biochem. J.*, 2004, **377**, 709-716.
16. S. Luca, W. M. Yau, R. Leapman and R. Tycko, *J. Biochem.*, 2007, **46**, 13505-13522.
17. G. T. Westermark, P. Westermark, C. Berne, O. Korsgren and T. Nordic Network Clin Islet, *New Engl. J. Med.*, 2008, **359**, 977-979.
18. M. R. Nilsson, M. Driscoll and D. P. Raleigh, *Protein Sci.*, 2002, **11**, 342-349.
19. E. B. Dunkelberger, L. E. Buchanan, P. Marek, P. Cao, D. P. Raleigh and M. T. Zanni, *J. Am. Chem. Soc.*, 2012, **134**, 12658-12667.
20. L. Haataja, T. Gurlo, C. J. Huang and P. C. Butler, *Endocr. Rev.*, 2008, **29**, 303-316.
21. A. Clark, C. Wells, I. Buley, J. Cruickshank, R. Vanhegan, D. Matthews, G. Cooper, R. Holman and R. Turner, *Diabetes research (Edinburgh, Scotland)*, 1988, **9**, 151-159.
22. A. Lorenzo, B. Razzaboni, G. C. Weir and B. A. Yankner, *Nature*, 1994, **368**, 756-760.
23. K. Potter, A. Abedini, P. Marek, A. Klimek, S. Butterworth, M. Driscoll, R. Baker, M. Nilsson, G. Warnock and J. Oberholzer, *Proc. Natl. Acad. Sci. USA*, 2010, **107**, 4305-4310.
24. P. T. Nguyen, X. Zottig, M. Sebastiao and S. Bourgault, *J. Biochem.*, 2017, **56**, 3808-3817.
25. R. Akter, P. Cao, H. Noor, Z. Ridgway, L. H. Tu, H. Wang, A. G. Wong, X. X.

- Zhang, A. Abedini, A. M. Schmidt and D. P. Raleigh, *J. Diabetes Res.*, 2016, DOI: 10.1155/2016/2798269, 18.
26. W. Y. K. Chan, T. D. Chan and P. B. O'Connor, *J. Am. Soc. Mass. Spectrom.*, 2010, **21**, 1012-1015.
  27. P. P. Hurtado and P. B. O'Connor, *Anal. Chem.*, 2012, **84**, 3017-3025.
  28. X. Li, X. Yu, C. E. Costello, C. Lin and P. B. O'Connor, *Anal. Chem.*, 2012, **84**, 6150-6157.
  29. J. J. Cournoyer, C. Lin, M. J. Bowman and P. B. O'Connor, *J. Am. Soc. Mass. Spectrom.*, 2007, **18**, 48-56.
  30. H. Yang and R. A. Zubarev, *Electrophoresis*, 2010, **31**, 1764-1772.
  31. N. E. Robinson and A. B. Robinson, *Proc. Natl. Acad. Sci. U. S. A.*, 2001, **98**, 4367-4372.
  32. Y. P. Y. Lam, C. A. Wootton, I. Hands-Portman, J. Wei, C. K. C. Chiu, I. Romero-Canelon, F. Lermyte, M. P. Barrow and P. B. O'Connor, *Anal. Chem.*, 2018, **Submitted**.
  33. P. Caravatti and M. Allemann, *Org. Mass Spectrom.*, 1991, **26**, 514-518.
  34. F. T. S. Chan, G. S. K. Schierle, J. R. Kumita, C. W. Bertoncini, C. M. Dobson and C. F. Kaminski, *Analyst*, 2013, **138**, 2156-2162.
  35. T. Yang, X. H. Wang, C. L. Zhang, X. Ma, K. Wang, Y. Q. Wang, J. Luo, L. Yang, C. Yao and X. Y. Wang, *Chem. Commun.*, 2016, **52**, 2245-2248.



### Graphic Abstracts:

Deamidation sites of hIAPP were determined and the amount of fibril formed in mutant hIAPPs were higher than wild-type hIAPP.

## **Electronic Supplementary Information**

### **Experimental Procedure**

**Sample preparation for deamidated hIAPP and fibrils.** Wild-type hIAPP lyophilized powder (Sigma Aldrich Company Ltd, Dorset, England) was dissolved in Milli-Q (Direct-Q® 3 UV System, Millipore Corporation, US) H<sub>2</sub>O (~pH 7.5) at a concentration of 500 µM and further diluted into 10 µM solution. The 10 µM hIAPP aqueous solution was incubated for 28 days (4 weeks). The incubated solution was then centrifuged at 14,000 rpm for one hour to separate the soluble hIAPP (supernatant) from the insoluble hIAPP fibril (fibrillary pellet). The supernatant solution containing soluble hIAPP was then diluted 20-fold with 49.5:49.5:1 water/acetonitrile/formic acid prior to MS analysis. hIAPP fibrillary pellets from 7-, 14-, 21-, and 28-day solutions were rinsed with 100 µL Milli-Q H<sub>2</sub>O three times and then re-dissolved with 20 µL of 47.5:47.5:5 water/acetonitrile/formic acid, and sonicated in water bath at 37 °C for one hour. Re-dissolved samples were further diluted with 80 µL of 50:50 water/acetonitrile. The final concentration of formic acid in solutions was 1% (mol/mol).

**Sample preparation for seeding mutant peptides.** Wild-type hIAPP lyophilized powder and synthetic mutant hIAPPs (Pepscan Company Ltd, The Netherlands) were dissolved in Milli-Q H<sub>2</sub>O to a concentration of 500 µM. The seeding experiments were performed by mixing wild-type hIAPP stock solution with 5%, 10%, 25%, or 50% mutant ((D)<sub>3</sub>hIAPP) or ((isoD)<sub>3</sub>hIAPP) solutions. Samples were then diluted to a final concentration of 10 µM wild-type hIAPP plus mutant ((D)<sub>3</sub>hIAPP) or ((isoD)<sub>3</sub>hIAPP), which were incubated for 1 week at 37°C. The supernatants and fibrillary pellets were separated and prepared as mentioned above.

**FTICR MS analysis.** Mass spectra were acquired on a 12 tesla solarix FTICR MS (Bruker Daltonik GmbH, Bremen, Germany). All samples were analyzed in positive ionization mode. For the detection of deamidated hIAPP and dissociated fibrils, an Apollo II electrospray ionization (ESI) source (Bruker Daltonik GmbH, Bremen, Germany) was used with a capillary voltage of 4-4.5 kV. The ESI flow rate was optimized to 100-150 µL/h and the source temperature was set to 200°C. Ions were externally accumulated in a hexapole collision cell before transferred to an infinity cell (ICR cell) for excitation and detection.<sup>33</sup> Data obtained from FTICR-MS were analyzed using Bruker DataAnalysis 4.2 software (Bruker Daltonics, Bremen, Germany). For the CAD experiments, precursor ions were first isolated using the quadrupole mass filter, then collided with argon gas and accumulated in the collision cell. The collision energy was optimized to 2-18 V and the ion accumulation time to

1-3 seconds. Fragments were then transferred to the infinity cell for detection. The most intense isotopic peak from each fragment with signal-to-noise ratio (S/N) over 5 was manually matched with the theoretical  $m/z$ . All of the fragments were internally calibrated and then assigned with an uncertainty less than 1 part-per-million (ppm).

**Quantification of deamidated/ mutant hIAPP in solutions and fibrillary pellets.**

The monoisotopic peak area of non-deamidated and deamidated/mutant hIAPP peaks were measured using Bruker DataAnalysis 4.2 software. The percentage of deamidated hIAPP (%) was calculated as follows:

$$\text{Deamidated (\%)} = \frac{\text{Peak area of deamidated hIAPP}}{\text{Sum of Peak area of deamidated hIAPP and nondeamidated hIAPP}} \times 100\%$$

The same calculation method was applied to obtain the percentage of mutant hIAPP against wild-type hIAPP.

**Transmission electron microscopy (TEM).** The TEM images of the incubated solutions, including 10  $\mu\text{M}$  wild-type hIAPP, 10  $\mu\text{M}$  mutant ((D)<sub>3</sub>hIAPP), and 10  $\mu\text{M}$  mutant ((isoD)<sub>3</sub>hIAPP) solution were acquired on a Jeol 2010F TEM operated at 200 kV. 10  $\mu\text{L}$  of incubated solution was transferred onto a carbon-coated grid and settled for one minute, followed by removing the excess solution using filter paper. A 2% (w/v) uranyl acetate solution was used for the negative stain. Multiple images with magnification from x10,000 to x40,000 were acquired.

**Thioflavin T (ThT) fluorescence reactivity.** The fluorescence reactivity of the 10  $\mu\text{M}$  hIAPP, mutant ((D)<sub>3</sub>hIAPP), mutant ((isoD)<sub>3</sub>hIAPP), and hIAPP seeding solutions were measured using a GloMax®-Multi Detection System (Promega; Wisconsin, USA). All samples were placed in a black 96 well-plate and mixed with 10  $\mu\text{M}$  ThT aqueous solution. Fluorescence spectra of the samples were acquired every 45 minutes with excitation at 405 nm and emission measurement at 490 nm, in a similar fashion to Chan *et al.*<sup>34, 35</sup> The intensities obtained from the fluorescence spectrometer were normalized to the signal intensity of the most mature fibril.

Deamidated (D)<sub>3</sub>hIAPP: KCNTATCATQRLANFLVHSS **DD**FGAILSST NVGS**D**TY-NH<sub>2</sub>

Deamidated (isoD)<sub>3</sub>hIAPP: KCNTATCATQRLANFLVHSS **(isoD)(isoD)**FGAILSST NVGS**(isoD)**TY-NH<sub>2</sub>

**Figure S1.** Sequences of synthetic mutant hIAPPs. Asn residues at position 21, 22, and 35 are replaced with aspartic acid – deamidated ((D)<sub>3</sub>hIAPP) or iso-aspartic acid – deamidated ((isoD)<sub>3</sub>hIAPP) in order to act as deamidation mimics.



**Monomer Cleavages detected:**

Monomer a ion  
Monomer c ion

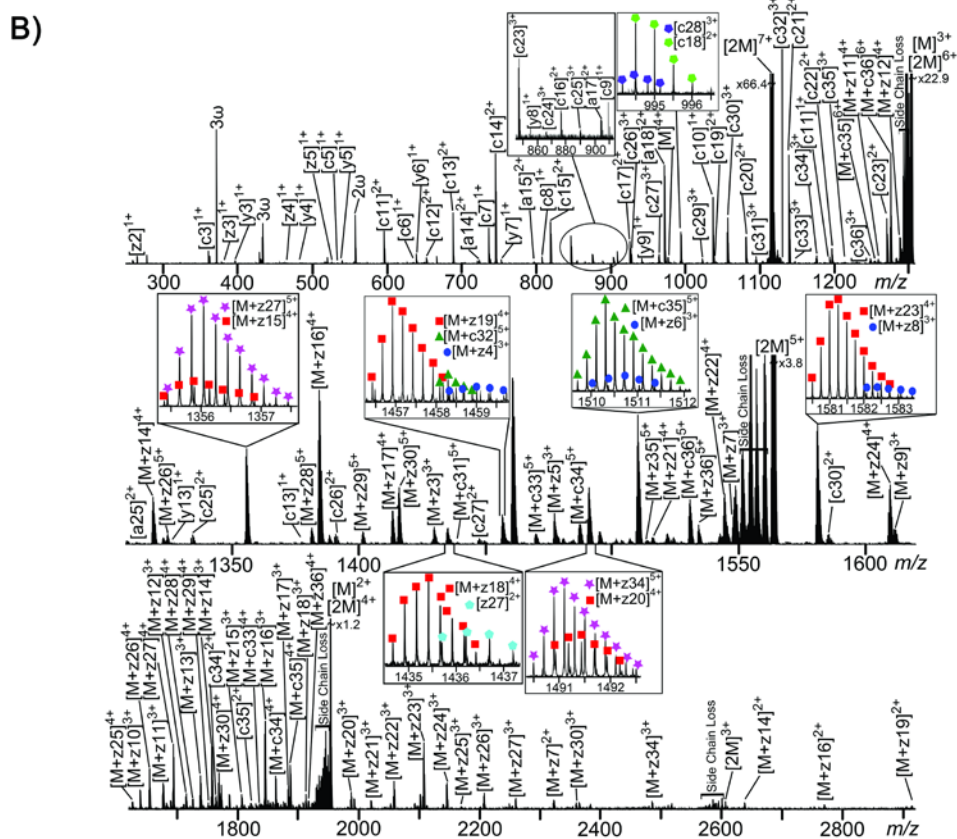
K C N T A T C A T Q R L A N F L V H S S D D F G A I L S S T N V G S D T Y - N H <sub>2</sub>

**Dimer Cleavages detected:**

Dimer c ion

K C N T A T C A T Q R L A N F L V H S S D D F G A I L S S T N V G S D T Y - N H <sub>2</sub>

Dimer z ion



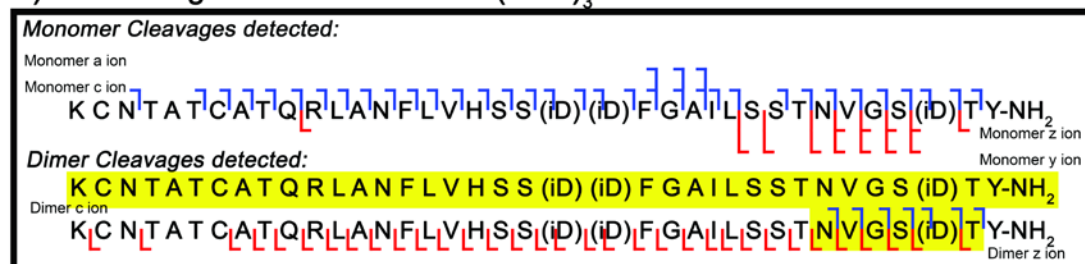
15

## Assignment Table of the ECD MS/MS of 7+ charge state ((D)<sub>3</sub>hIAPP) dimer

Ion	charge	Theoretical m/z	Experimental m/z	Error (ppm)	Ion	charge	Theoretical m/z	Experimental m/z	Error (ppm)
MH	4+	977.462474	977.461786	-0.704	M+c32	4+	1822.618557	1822.618598	0.022
MH	3+	1302.279143	1302.279165	0.017	M+c33	5+	1469.700594	1469.701214	0.422
MH	2+	1952.915077	1952.915991	0.468	M+c33	4+	1837.376472	1837.376990	0.282
2[MH]	7+	1116.383162	1116.383047	-0.103	M+c34	5+	1487.107000	1487.107008	0.005
2[MH]	6+	1303.115465	1303.115560	0.073	M+c34	4+	1858.883887	1858.885137	0.672
2[MH]	5+	1563.738667	1563.738999	0.212	M+c35	6+	1258.761936	1258.761197	-0.587
2[MH]	4+	1954.674371	1954.674185	0.365	M+c35	5+	1510.312868	1510.313214	0.229
2[MH]	3+	2605.897413	2605.897274	-0.053	M+c35	4+	1887.891222	1887.892061	0.444
a14	2+	724.354565	724.354485	-0.110	M+c36	6+	1275.603219	1275.603240	0.016
a15	2+	797.888772	797.888565	-0.259	M+c36	5+	1530.924420	1530.924741	0.210
a17	2+	903.965011	903.965096	0.094	M+z3	3+	1429.328685	1429.329245	0.392
a18	2+	972.494467	972.494518	0.052	M+z4	3+	1458.339361	1458.339476	0.079
a22	2+	1174.553438	1174.553758	0.272	M+z5	3+	1477.346514	1477.347034	0.352
a23	2+	1248.087645	1248.088012	0.294	M+z6	3+	1510.359320	1510.368816	-0.334
a25	2+	1312.116934	1312.116940	0.005	M+z7	3+	1548.049351	1548.049768	0.269
c3	1+	362.173076	362.173008	-0.188	M+z7	2+	2323.077144	2323.078314	0.504
c5	1+	534.257869	534.257735	-0.251	M+z8	3+	1582.400354	1582.401276	0.583
c6	1+	636.313372	636.313252	-0.189	M+z9	3+	1611.746974	1611.746129	-0.524
c7	1+	737.306908	737.306867	-0.056	M+z10	3+	1639.753258	1639.752527	-0.446
c8	1+	808.344022	808.344002	-0.025	M+z11	4+	1258.839125	1258.839009	-0.092
c9	1+	909.391701	909.391767	0.073	M+z11	3+	1677.447952	1677.448418	0.278
c10	1+	1037.450279	1037.450336	0.055	M+z12	4+	1287.110147	1287.110616	0.364
c11	2+	597.279333	597.279236	-0.162	M+z12	3+	1715.811104	1715.812415	0.764
c11	1+	1193.551390	1193.551711	0.269	M+z13	4+	1304.869427	1304.869520	0.071
c12	2+	653.821365	653.821279	-0.132	M+z13	3+	1738.821678	1738.820724	-0.549
c13	2+	689.339922	689.339851	-0.103	M+z14	4+	1318.623443	1318.623618	0.133
c13	1+	1377.672568	1377.673273	0.512	M+z14	3+	1757.828832	1757.829443	0.348
c14	2+	746.361386	746.361348	-0.051	M+z14	2+	2637.748852	2637.749391	0.204
c15	2+	819.895593	819.895538	-0.067	M+z15	4+	1355.390547	1355.390850	0.224
c16	2+	876.437625	876.437608	-0.019	M+z15	3+	1807.856058	1807.856916	0.475
c17	2+	925.971832	925.971879	0.051	M+z16	4+	1384.147283	1384.147298	0.011
c18	2+	994.501288	994.501285	-0.003	M+z16	3+	1846.532522	1846.533255	0.397
c19	2+	1038.017303	1038.017350	0.045	M+z16	2+	2769.799453	2769.799567	0.041
c20	2+	1081.533317	1081.533397	0.074	M+z17	4+	1412.904019	1412.904502	0.342
c21	2+	1139.046789	1139.046886	0.068	M+z17	3+	1884.874843	1884.874962	0.063
c22	2+	1196.560261	1196.560497	0.197	M+z18	4+	1434.912737	1434.913034	0.207
c23	3+	847.065404	847.065401	-0.004	M+z18	3+	1913.895523	1913.895817	0.154
c23	2+	1270.094468	1270.094648	0.142	M+z19	4+	1456.420033	1456.420138	0.072
c24	3+	866.072559	866.072757	0.229	M+z19	3+	1942.896202	1942.895513	-0.355
c25	3+	889.751597	889.751369	-0.256	M+z19	2+	2914.846456	2914.846774	0.109
c25	2+	1334.123849	1334.123808	-0.031	M+z20	4+	1491.186124	1491.186700	0.386
c26	3+	927.446285	927.446297	0.013	M+z20	3+	1988.582507	1988.583390	0.444
c26	2+	1390.665789	1390.665948	0.114	M+z21	4+	1515.953231	1515.953433	0.133
c27	3+	965.140973	965.141253	0.290	M+z21	3+	2021.605320	2021.606146	0.409
c27	2+	1447.709221	1447.709709	0.337	M+z22	4+	1544.224252	1544.224820	0.368
c28	3+	994.151649	994.151665	0.016	M+z22	3+	2059.300020	2059.301231	0.588
c29	3+	1023.162325	1023.162402	0.075	M+z23	4+	1580.489984	1580.490360	0.238
c29	2+	1535.242655	1535.243476	0.535	M+z23	3+	2108.322843	2108.323867	0.486
c30	3+	1056.844885	1056.844929	0.042	M+z24	4+	1609.000716	1609.001073	0.222
c30	2+	1584.763690	1584.764560	0.549	M+z24	3+	2146.337153	2146.338370	0.567
c31	3+	1094.859194	1094.859257	0.058	M+z25	4+	1627.512008	1627.512728	0.442
c31	2+	1642.286550	1642.287622	0.653	M+z25	3+	2170.350335	2170.351553	0.561
c32	3+	1127.881999	1127.882005	0.005	M+z26	5+	1324.827880	1324.828098	0.165
c32	2+	1692.823617	1692.824904	0.760	M+z26	4+	1655.783031	1655.783641	0.368
c33	3+	1146.889154	1146.889155	0.001	M+z26	3+	2208.046833	2208.046628	-0.093
c34	3+	1175.899830	1175.899842	0.010	M+z27	5+	1356.048099	1356.048275	0.130
c34	2+	1763.346107	1763.347520	0.801	M+z27	4+	1695.060261	1695.060689	0.252
c35	3+	1214.576411	1214.576892	0.396	M+z27	3+	2260.080530	2260.081089	0.247
c35	2+	1820.859579	1820.859880	0.154	M+z28	5+	1381.659815	1381.660080	0.192
c36	3+	1247.924704	1247.924446	-0.207	M+z28	4+	1726.824267	1726.824613	0.200
y3	1+	397.171777	397.171687	-0.227	M+z29	5+	1402.069844	1402.070205	0.257
y4	1+	484.203606	484.203654	-0.314	M+z29	4+	1752.086188	1752.086770	0.332
y5	1+	541.225270	541.225155	-0.212	M+z30	5+	1416.076777	1416.077014	0.167
y6	1+	640.293684	640.293629	-0.086	M+z30	4+	1770.096109	1770.096483	0.211
y7	1+	754.336612	754.336600	-0.016	M+z30	3+	2359.792401	2359.792212	-0.080
y8	1+	855.384291	855.384408	0.137	M+z34	5+	1491.103517	1491.103695	0.119
y9	1+	942.416320	942.416439	0.126	M+z34	4+	1864.130123	1864.130663	0.290
y10	1+	1029.448349	1029.448387	0.037	M+z34	3+	2485.507093	2485.507949	0.344
y13	1+	1326.653591	1326.653604	0.010	M+z35	5+	1513.912103	1513.912030	-0.048
z2	1+	266.126109	266.126109	0.000	M+z36	5+	1534.713228	1534.713352	0.081
z3	1+	382.160877	382.160842	-0.092	M+z36	4+	1918.141132	1918.141936	0.419
z4	1+	467.177255	467.177105	-0.321					
z5	1+	526.214369	526.214234	-0.257					
z27	2+	1435.701402	1435.700996	-0.283					
M+c31	5+	1438.883524	1438.884166	0.446					
M+c32	5+	1458.496774	1458.496281	-0.338					
					Average Error:				0.124
					Absolute Average Error:				0.236
					Standard Deviation:				0.278

**Table S1.** List of the assigned fragments from the ECD MS/MS spectrum of the 7+ charge state ((D)<sub>3</sub>hIAPP) dimer ion. M represents one ((D)<sub>3</sub>hIAPP) unit.

# A) ECD Fragmentation of the 7+ (isoD)<sub>3</sub>hIAPP Dimer



B)

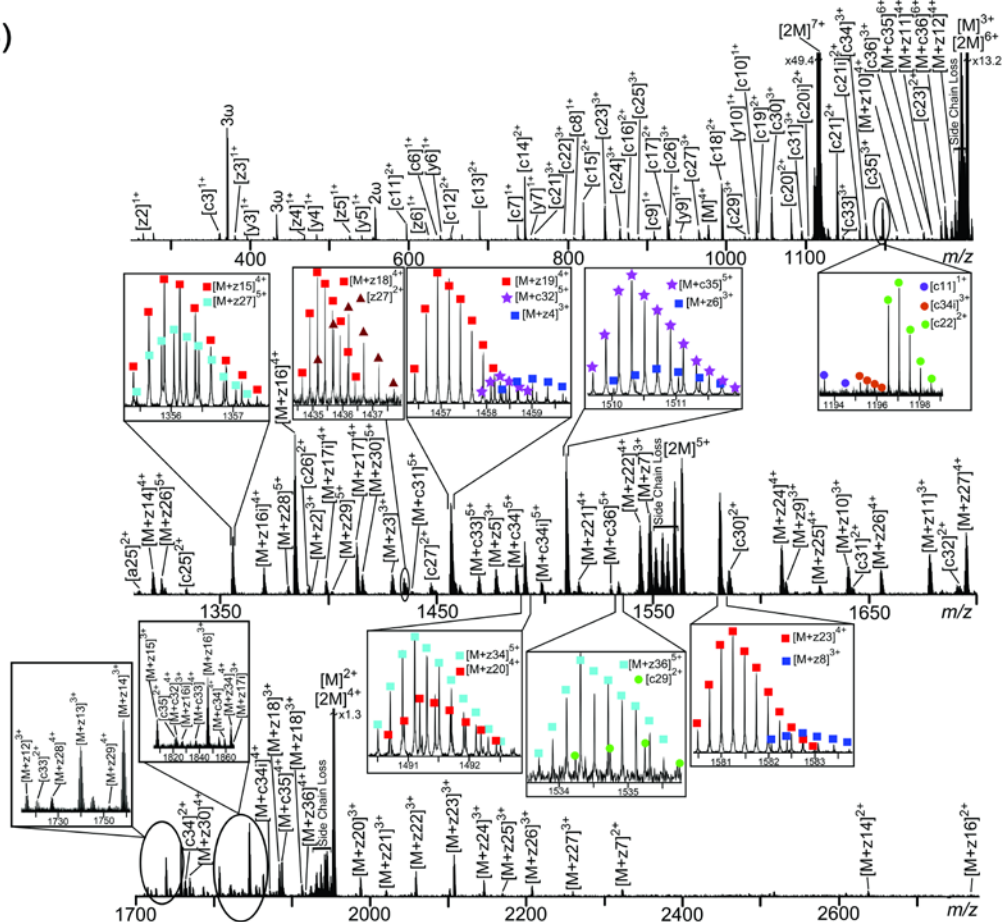


**Figure S3.** (A) Summary of a-, c-, y-, and z-ion fragments observed in the (B) ECD MS/MS spectrum of the 7+ charge state ((isoD)<sub>3</sub>hIAPP) dimer. Highlighted sequence represents the proposed non-covalent interaction region. The side chain losses were not labeled for clarity. The assigned fragments are listed in the ESI Table S2.

## Assignment Table of the ECD MS/MS of 7+ charge state ((isoD)<sub>3</sub>hIAPP) dimer

Type	Ion	charge	Theoretical m/z	Experimental m/z	Error (ppm)	Type	Ion	charge	Theoretical m/z	Experimental m/z	Error (ppm)
MH	MH	4+	977.211884	977.211677	-0.212	M+c	34	5+	1487.105911	1487.106523	0.412
MH	MH	3+	1302.279143	1302.279080	-0.048	M+c	34	4+	1858.883887	1858.883845	-0.023
MH	MH	2+	1952.915077	1952.915655	0.296	M+c	35	6+	1258.761936	1258.761954	0.014
2[MH]	2[MH]	7+	1116.383162	1116.383218	0.050	M+c	35	5+	1510.312868	1510.312981	0.075
2[MH]	2[MH]	6+	1303.115465	1303.115597	0.101	M+c	35	4+	1887.891222	1887.891506	0.150
2[MH]	2[MH]	5+	1563.738657	1563.738713	0.029	M+c	36	6+	1275.603219	1275.603316	0.076
2[MH]	2[MH]	4+	1954.673471	1954.672757	-0.365	M+c	36	5+	1530.524420	1530.524203	-0.142
a	23	2+	1248.087645	1248.087793	0.119	M+c	34i	5+	1498.707009	1498.707619	0.407
a	24	2+	1277.099772	1277.099889	0.092	M+c	34i	4+	1873.131943	1873.132905	0.514
a	25	2+	1312.116934	1312.117109	0.133	M+z	2	3+	1391.654617	1391.655808	0.856
c	3	1+	362.173076	362.173033	-0.119	M+z	3	3+	1429.328685	1429.329444	0.531
c	6	1+	636.313372	636.313275	-0.152	M+z	4	3+	1458.339361	1458.340006	0.442
c	7	1+	737.306908	737.306876	-0.043	M+z	5	3+	1477.680667	1477.680895	0.154
c	8	1+	808.344022	808.343966	-0.069	M+z	6	3+	1510.369320	1510.368775	-0.361
c	9	1+	909.391701	909.391605	-0.106	M+z	7	3+	1548.049351	1548.049654	0.196
c	10	1+	1037.450279	1037.450277	-0.002	M+z	7	2+	2323.578098	2323.578660	0.242
c	11	2+	597.279333	597.279315	-0.030	M+z	8	3+	1582.400354	1582.401094	0.468
c	11	1+	1193.551390	1193.551247	-0.120	M+z	9	3+	1611.746974	1611.746700	-0.170
c	12	2+	653.821365	653.821303	-0.095	M+z	10	4+	1230.568102	1230.567991	-0.090
c	13	2+	689.339922	689.339931	0.013	M+z	10	3+	1639.753258	1639.753036	-0.135
c	14	2+	746.361386	746.361372	-0.019	M+z	11	4+	1268.839125	1268.839593	0.372
c	15	2+	819.895593	819.895597	0.005	M+z	11	3+	1677.447952	1677.447828	-0.074
c	16	2+	876.437625	876.437697	0.062	M+z	12	4+	1287.110147	1287.110909	0.592
c	17	2+	925.971832	925.971846	0.015	M+z	12	3+	1715.811104	1715.811618	0.300
c	18	2+	964.501288	964.501292	0.004	M+z	13	4+	1304.869427	1304.869611	0.141
c	19	2+	1038.017303	1038.017376	0.070	M+z	13	3+	1738.821678	1738.821082	-0.343
c	20	2+	1081.533317	1081.533351	0.031	M+z	14	4+	1318.623443	1318.623189	-0.193
c	21	3+	759.700285	759.700251	-0.045	M+z	14	3+	1757.828832	1757.829081	0.142
c	21	2+	1139.046789	1139.046820	0.027	M+z	14	2+	2638.247419	2638.246892	-0.200
c	22	3+	798.042599	798.042537	-0.078	M+z	15	4+	1355.390547	1355.390795	0.183
c	22	2+	1196.560261	1196.560293	0.027	M+z	15	3+	1807.856058	1807.856380	0.178
c	23	3+	847.065404	847.065386	-0.021	M+z	16	4+	1384.147283	1384.147411	0.092
c	23	2+	1270.094468	1270.094418	-0.039	M+z	16	3+	1846.532522	1846.532903	0.206
c	24	3+	866.072559	866.072652	0.107	M+z	16	2+	2769.295145	2769.294672	-0.171
c	25	3+	889.751597	889.751696	0.111	M+z	17	4+	1412.904019	1412.903882	-0.097
c	25	2+	1334.123849	1334.123757	-0.069	M+z	17	3+	1884.874843	1884.874708	-0.072
c	26	3+	927.446285	927.446286	0.001	M+z	18	4+	1434.912737	1434.912984	0.172
c	26	2+	1390.685789	1390.686501	0.512	M+z	18	3+	1913.885523	1913.885178	-0.180
c	27	3+	965.140873	965.140983	0.110	M+z	19	4+	1456.420033	1456.420238	0.141
c	27	2+	1447.709221	1447.709778	0.385	M+z	19	3+	1942.896202	1942.895988	-0.110
c	29	3+	1023.162325	1023.162215	-0.108	M+z	20	4+	1491.186124	1491.186435	0.209
c	29	2+	1534.239850	1534.239965	0.075	M+z	20	3+	1988.582507	1988.582942	0.219
c	30	3+	1056.844885	1056.844848	-0.035	M+z	21	4+	1515.953231	1515.953379	0.098
c	30	2+	1584.763690	1584.763724	0.021	M+z	21	3+	2021.805320	2021.805553	0.115
c	31	3+	1094.859184	1094.859270	0.069	M+z	22	4+	1544.224252	1544.224504	0.163
c	31	2+	1642.787956	1642.788594	0.388	M+z	22	3+	2059.300020	2059.300910	0.432
c	32	3+	1127.881999	1127.881584	-0.368	M+z	23	4+	1580.489984	1580.489808	-0.111
c	32	2+	1691.319356	1691.320699	0.794	M+z	23	3+	2108.322843	2108.323448	0.287
c	33	3+	1146.889154	1146.888901	-0.221	M+z	24	4+	1609.000716	1609.000938	0.138
c	33	2+	1720.331490	1720.332143	0.380	M+z	24	3+	2146.337153	2146.337709	0.259
c	34	3+	1175.899830	1175.899636	-0.165	M+z	25	4+	1627.512008	1627.512645	0.391
c	34	2+	1763.346107	1763.346490	0.217	M+z	25	3+	2170.350335	2170.351009	0.311
c	35	3+	1214.576411	1214.576568	0.129	M+z	26	5+	1324.827880	1324.827646	-0.177
c	35	2+	1820.859579	1820.860110	0.292	M+z	26	4+	1655.783031	1655.783415	0.232
c	36	3+	1247.924704	1247.924462	-0.194	M+z	26	3+	2208.046833	2208.046104	-0.330
c	20i	2+	1110.032142	1110.032427	0.256	M+z	27	5+	1356.048099	1356.048495	0.292
c	21i	2+	1167.545613	1167.545686	0.063	M+z	27	4+	1695.060261	1695.060550	0.170
c	34i	3+	1195.233316	1195.233951	0.531	M+z	27	3+	2260.080530	2260.081289	0.336
y	3	1+	397.171777	397.171827	0.126	M+z	28	5+	1381.659815	1381.660250	0.315
y	4	1+	484.203806	484.203771	-0.072	M+z	28	4+	1726.524267	1726.523766	-0.290
y	5	1+	541.225270	541.225281	0.020	M+z	29	5+	1402.069844	1402.069738	-0.076
y	6	1+	640.293684	640.293709	0.039	M+z	29	4+	1752.086188	1752.086786	0.341
y	7	1+	754.336812	754.336583	-0.065	M+z	30	5+	1416.076777	1416.076531	-0.174
y	9	1+	942.416320	942.416353	0.035	M+z	30	4+	1769.844153	1769.844536	0.216
y	10	1+	1029.448349	1029.448645	0.288	M+z	34	5+	1491.103517	1491.103470	-0.032
z	2	1+	266.126109	266.126109	0.000	M+z	34	4+	1864.130123	1864.130353	0.123
z	3	1+	382.160877	382.160841	-0.094	M+z	36	5+	1534.713228	1534.713224	-0.003
z	4	1+	469.192905	469.192914	0.019	M+z	36	4+	1918.141132	1918.141912	0.407
z	5	1+	526.214369	526.214338	-0.059	M+z	16-i	4+	1370.399228	1370.399399	0.125
z	6	1+	625.282783	625.282678	-0.168	M+z	16-i	3+	1827.199153	1827.199447	0.161
z	27	2+	1435.197489	1435.196299	-0.829	M+z	17-i	4+	1399.406577	1399.406737	0.114
M+c	31	5+	1438.482615	1438.482645	0.021	M+z	17-i	3+	1865.875642	1865.875456	-0.100
M+c	32	4+	1822.618557	1822.618534	-0.013	Average Error:					0.068
M+c	33	5+	1469.700594	1469.699673	-0.627	Absolute Average Error:					0.187
M+c	33	4+	1837.375068	1837.375877	0.440	Standard Deviation:					0.245

**Table S2.** List of the assigned fragments from the ECD MS/MS spectrum of the 7+ charge state ((isoD)<sub>3</sub>hIAPP) dimer ion. M represents one ((isoD)<sub>3</sub>hIAPP) unit.



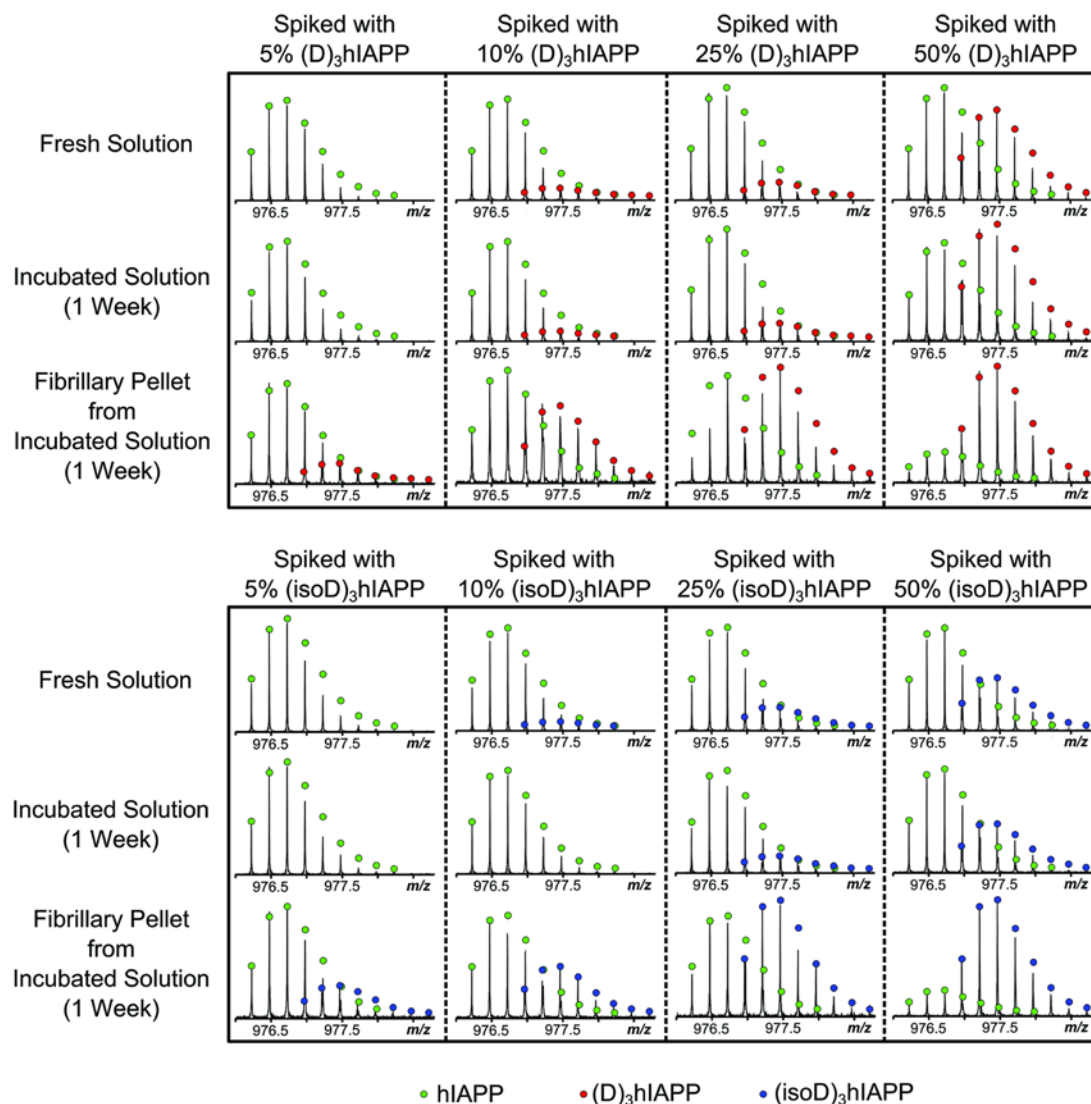


**Figure S4.** The nESI-MS spectra showing the fresh, the incubated solutions, and the incubated fibrillary pellets of hIAPP mixed with 5%, 10%, 25%, or 50% of mutant ((D)<sub>3</sub>hIAPP) or ((isoD)<sub>3</sub>hIAPP).